AGU PUBLICATIONS

JGR

Journal of Geophysical Research: Space Physics

RESEARCH ARTICLE
10.1002/2016JA022832

Special Section:
Geospace system responses to the St. Patrick's Day storms in 2013 and 2015

Effects of disturbed electric fields in the low-latitude and equatorial ionosphere during the 2015 St. Patrick's Day storm

Jiawei Kuai[1,2,3], Libo Liu[1,2,3], Jing Liu[4], S. Sripathi[5], Biqiang Zhao[1,2], Yiding Chen[1,2], Huijun Le[1,2], and Lianhuan Hu[1,2]

[1]Key Laboratory of Earth and Planetary Physics, Institute of Geology and Geophysics, Chinese Academy of Sciences, Beijing, China, [2]Beijing National Observatory of Space Environment, Institute of Geology and Geophysics, Chinese Academy of Sciences, Beijing, China, [3]University of Chinese Academy of Sciences, Beijing, China, [4]High Altitude Observatory, National Center for Atmospheric Research, Boulder, Colorado, USA, [5]Indian Institute of Geomagnetism, Mumbai, India

Key Points:
- The disturbed electric fields play a decisive role in the ionospheric responses in low latitude and equatorial regions during the storm
- Penetration electric fields and disturbance dynamo electric fields occur in both the Asian-Australian sector and the American sector
- The salient storm time F3 layer is observed in the American equatorial region but not in the East Asian sector

Correspondence to:
L. Liu,
liul@mail.iggcas.ac.cn

Citation:
Kuai, J., L. Liu, J. Liu, S. Sripathi, B. Zhao, Y. Chen, H. Le, and L. Hu (2016), Effects of disturbed electric fields in the low-latitude and equatorial ionosphere during the 2015 St. Patrick's Day storm, *J. Geophys. Res. Space Physics*, *121*, doi:10.1002/2016JA022832.

Received 19 APR 2016
Accepted 30 AUG 2016
Accepted article online 2 SEP 2016

Abstract The 2015 St. Patrick's Day geomagnetic storm with *SYM-H* value of −233 nT is an extreme space weather event in the current 24th solar cycle. In this work, we investigated the main mechanisms of the profound ionospheric disturbances over equatorial and low latitudes in the Asian-Australian sector and the American sector during this super storm event. The results reveal that the disturbed electric fields, which comprise penetration electric fields (PEFs) and disturbance dynamo electric fields (DDEFs), play a decisive role in the ionospheric storm effects in low latitude and equatorial regions. PEFs occur on 17 March in both the American sector and the Asian-Australian sector. The effects of DDEFs are also remarkable in the two longitudinal sectors. Both the DDEFs and PEFs show the notable local time dependence, which causes the sector differences in the characteristics of the disturbed electric fields. This differences would further lead to the sector differences in the low-latitude ionospheric response during this storm. The negative storm effects caused by the long-duration DDEFs are intense over the Asian-Australian sector, while the repeated elevations of h_mF_2 and the equatorial ionization anomaly intensifications caused by the multiple strong PEFs are more distinctive over the American sector. Especially, the storm time F_3 layer features are caught on 17 March in the American equatorial region, proving the effects of the multiple strong eastward PEFs.

1. Introduction

During geomagnetic storms, solar wind energy being coupled into the ionosphere is significantly enhanced, driving considerable changes in the compositions, temperature, circulation, and electric fields of the whole thermosphere-ionosphere (*T-I*) system. Ionospheric storms represent the extreme state of the ionosphere caused by geomagnetic storms. As a result, significant changes in total electron content (TEC) and the electron densities are caused by these disturbances during geomagnetic storms. Compared with geomagnetically quiet conditions, the enhancements and depletions in ionospheric electron densities/TEC are known as positive and negative ionospheric storm effects, respectively.

Being considered as the most complicated phenomena in the *T-I* system, ionospheric storms have been investigated as a hot spot for several decades [*Prölss*, 2008; *Liu and Wan*, 2016], and various features of the ionospheric response to geomagnetic storms have been revealed by observations and simulations [e.g., *Prölss*, 1995; *Abdu*, 1997; *Buonsanto*, 1999; *Danilov and Lăstovička*, 2001; *Liu et al.*, 2004; *Mendillo*, 2006; *Burns et al.*, 2007; *Prölss*, 2008; *Danilov*, 2013; *Liu et al.*, 2014; *Suvorova et al.*, 2014].

Remarkable variations of the compositions, thermodynamics, and electrodynamics in the *T-I* system can be the sources to drive the storm time ionospheric effects during geomagnetic storms. The movement and evolvement of the neutral composition disturbance (decreased [O]/[N_2]) zone would alter the electron densities in the ionospheric *F* region during geomagnetic storms [*Burns et al.*, 1989; *Prölss*, 1995]. Dynamic processes in the form of large-scale thermospheric circulation or traveling atmospheric disturbances also play a significant role in the plasma redistribution [*Habarulema et al.*, 2015]. For example, the disturbed equatorward neutral winds will push the F_2 layer to higher altitudes where the recombination rates are lower so that the electron densities tend to increase. The equatorward neutral winds could also hinder the formation of equatorial ionization anomaly (EIA) and then cause the positive storm effects in the equatorial regions and negative ionospheric storm effects in the crest regions [*Prölss*, 1995].

In low latitude and equatorial regions, the storm time ionospheric disturbed electric fields are a particularly important contributor to ionospheric storm effects. The disturbed electric fields can affect the occurrence of plasma density irregularities and redistribute the ionospheric plasma to create ionospheric storm effects in low latitude and equatorial regions [e.g., *Fejer*, 1986; *Abdu*, 1997; *Sastri et al.*, 2000; *Bagiya et al.*, 2011; *Kuai et al.*, 2015; *Carter et al.*, 2016]. Generally speaking, the disturbed electric fields can be grouped into two categories: penetration electric fields (PEFs) and disturbance dynamo electric fields (DDEFs). The PEF is thought as the penetration of solar wind motional electric field into the ionosphere. PEFs are highly correlated with interplanetary magnetic field B_z component and normally are short-lived [e.g., *Fejer*, 1997; *Huang et al.*, 2005; *Wei et al.*, 2011, 2015]. In general, on the dayside ionosphere, the southward turning of interplanetary magnetic field (IMF) B_z may lead to an eastward PEF (undershielding), and an abrupt northward turning after southward IMF will result in a westward PEF (overshielding). The DDEF comes from the ionospheric disturbance dynamo effects due to the enhanced energy injection into the auroral altering the global circulation and the generation of electric fields and currents. The DDEF is westward on the dayside and eastward on the nightside, i.e., opposite to the direction of ionospheric dynamo electric fields. Further, the DDEF is long-lived and more slowly varying, compared to PEFs [e.g., *Blanc and Richmond*, 1980; *Fejer et al.*, 1983; *Sastri*, 1988; *Fejer*, 2011; *Bagiya et al.*, 2011].

The "case study" approach could enrich our understanding of the ionospheric storm effects and proposed mechanisms, especially for extreme space weather events [*Mendillo*, 2006]. The geomagnetic storm occurring on 17–20 March 2015, which is characterized by the minimum *SYM-H* value of −233 nT, is an extreme event of space weather in the current 24th solar cycle. This extreme space weather event has become a research focus for the ionospheric community most recently. *Astafyeva et al.* [2015] presented the global results of the complex ionospheric storm effects and highlighted the inverse hemispheric asymmetries in the ionospheric response during the great geomagnetic storm. *Ramsingh et al.* [2015] analyzed the ionospheric response and reported the storm-induced plasma density irregularities/scintillations over Indian sector. *Liu et al.* [2016] investigated a large-scale and local view of a storm-enhanced density (SED) event during the main phase of the great storm and found that the SED occurred where there was a negative phase near the F_2 peak and a positive phase in the topside ionosphere. These studies have revealed many salient features for this great ionospheric storm event.

However, the profound ionospheric disturbances and the main mechanisms in low latitude and equatorial regions are complex and still not clear during the March 2015 storm. Simultaneously, the sector differences in the low-latitude ionospheric responses and the corresponding controlling factors are also issues worthy of attention for the great event. Therefore, we will focus on the ionospheric storm effects and investigate the related mechanisms in low latitude and equatorial regions in both the Asian-Australian sector and the American sector during the 17–20 March 2015 event in this work. More importantly, the prominent role of the disturbed electric fields, which comprise penetration electric fields (PEFs) and disturbance dynamo electric fields (DDEFs), will be discussed and contrasted in low latitude and equatorial regions in the two longitudinal sectors during this event.

2. Data Presentation

The solar wind parameters come from the OMNIWeb database [*King and Papitashvili*, 2005], and these data are obtained from the Advanced Composition Explorer satellite measurements. The *AE* index roughly indicates the auroral energy inputs, the symmetric component of ring current (*SYM-H*) index can be regarded as a high-resolution version of the *Dst* index [*Wanliss and Showalter*, 2006], and the *Kp* index can be used to describe geomagnetic conditions at midlatitudes. The GPS TEC at a 5 min resolution are provided by the Massachusetts Institute of Technology Haystack Observatory Madrigal database [*Rideout and Coster*, 2006].

The ionospheric F_2 layer parameters are routinely scaled at five ionosonde stations gated in low latitude and equatorial regions. The ionosonde stations at Sanya (18.3°N, 109.6°E, 24.98° dip angle) and Guam (13.6°N, 144.9°E, 12.78° dip angle) are located in the Asian-Australian sector, and the stations at Jicamarca (12.0°S, 76.8°W, −0.48° dip angle), Sao Luis (2.6°S, 44.2°W, −7.06° dip angle), and Fortaleza (3.9°S, 38.4°W, −15.77° dip angle) are located in the American sector. We have manually scaled the ionograms and used the SAO-Explorer software package to obtain the F_2 layer critical frequency (f_oF_2) and F_2 layer peak height (h_mF_2) based on the built-in true height inversion algorithm [*Huang and Reinisch*, 1996].

Two pairs of magnetometers including equatorial and off-equatorial stations provide a measurement of the daytime equatorial electrojet and the intensity of the $\mathbf{E} \times \mathbf{B}$ drift in ionospheric *F* region [*Anderson et al.*, 2002]. In the Asian-Australian sector, the difference in the magnitudes of the geomagnetic horizontal (*H*) component ($\Delta H_{\text{cdo-mut}}$) between Cagayan De Oro (8.4°N, 124.6°E, 2.17° dip angle) and Muntinlupa (14.4°N, 121.0°E, 15.69° dip angle) is used for our analysis. In the American sector, another pair of magnetometers, including equatorial station Jicamarca (12.0°S, 76.8°W, −0.48° dip angle) and the off-equatorial station Leticia (4.1°S, 69.9°W, 12.66° dip angle), are used to measure the horizontal component difference ($\Delta H_{\text{jic-let}}$).

As a supplement, drift data over Indian sector are also utilized in our work. The ionospheric parameters are obtained from the Canadian Advanced Digital Ionosonde operating at an equatorial station Tirunelveli (8.7°N, 77.7°E). The Doppler drift mode observations at Tirunelveli are operated continuously at 1 min interval [*Ramsingh et al.*, 2015].

3. Results and Discussion

3.1. Solar Wind, IMF, and Geomagnetic Conditions During the March 2015 Storm

Figure 1 shows the variations of interplanetary magnetic field (IMF) B_z component (in nT), solar wind speed *V* (km/s), interplanetary electric field (IEF) E_y component (mV/m), *AE* index (nT), *SYM-H* index (nT), and *Kp* index during 16–20 March 2015.

On 16 March 2015, the day prior to the storm onset, the IMF B_z (in GSM coordinates) is mostly northward, the geomagnetic indices all are relatively small and stable, and the solar wind speed has a nonsignificant increase during the day, so this day can be regarded as the quiet time reference for this geomagnetic storm. Figure 1 gives the onset of the intense storm at about 04:45 UT on 17 March, when an interplanetary shock hits the Earth's magnetosphere. The IMF B_z turns northward for a while, the solar wind speed increases abruptly from ~400 to ~500 km/s, and a step-like increase in the *SYM-H* index indicates the trigger of sudden storm commencement. The IMF B_z turns southward at around 06:00 UT, the *AE* index has a significant increase to ~1000 nT, and the *SYM-H* index starts to decline, which are identified as the onset of the main phase of the geomagnetic storm. After reaching to −20 nT, the IMF B_z begins to go back to northward for a brief time from ~09:00 UT to ~11:30 UT before its southward turning again. Especially, after that, the IMF B_z continues for a long duration (>12 h) in the southward direction with a magnitude of about −20 nT. At the same time, the *AE* index has a salient increase for the second time to ~2000 nT; the solar wind speed increases to the magnitude of about 600 km/s. A magnetic cloud is associated with the significant increase in the magnitude of IMF and a smooth change in the direction of IMF (see IMF B_z in Figure 1). A high-speed solar wind steam event is also associated with the magnetic cloud [*Liu et al.*, 2016]. The IEF E_y is varying between dawn and dusk as the variations of the IMF B_z during this time.

The *SYM-H* index reaches the minimum value of −233 nT at about 23:00 UT on 17 March. After that, the geomagnetic storm goes into the recovery phase on 18 March. On 18–20 March, the solar wind speed keeps at a relatively high level of about 550–700 km/s and the IMF B_z oscillates between northward and southward. It is most likely caused by the combined effect of the compression process of the high-speed solar wind steams and the magnetic cloud [*Fenrich and Luhmann*, 1998; *Kataoka et al.*, 2015; *Liu et al.*, 2016]. The *AE* index indicates that the auroral energy is still inputting during the recovery phase on 18–20 March, which can be considered as multiple substorms [*Ramsingh et al.*, 2015].

3.2. Low-Latitude Ionospheric Response in the Asian-Australian Sector

Figure 2 illustrates the storm time distributions of TEC (Figure 2, top) and the deviations of TEC (DTEC) (Figure 2, middle) from the reference values in the coordinates of universal time (UT) and geographic latitude in the longitude ~120°E and the variations of $\Delta H_{\text{cdo-mut}}$ (Figure 2, bottom) on 16–20 March 2015. The gray curve in Figure 2 (bottom) denotes the quiet time reference values derived from the mean values of $\Delta H_{\text{cdo-mut}}$ on 15–16 March. The mean TEC data of five international quiet days of the month are used as the reference values to obtain the DTEC. International Quiet Days (IQDs) are the days where the geomagnetic variations are a minimum in each month. It is appropriate to use the data of IQDs for removing the day-to-day variability and identifying the storm time changes in the ionospheric parameters (e.g., TEC, f_oF_2, and h_mF_2). In this work, the five IQDs of March 2015 that we used are 10, 30, 05, 14, and 09 March (http://www.ga.gov.au/oracle/geomag/iqd_form.jsp).

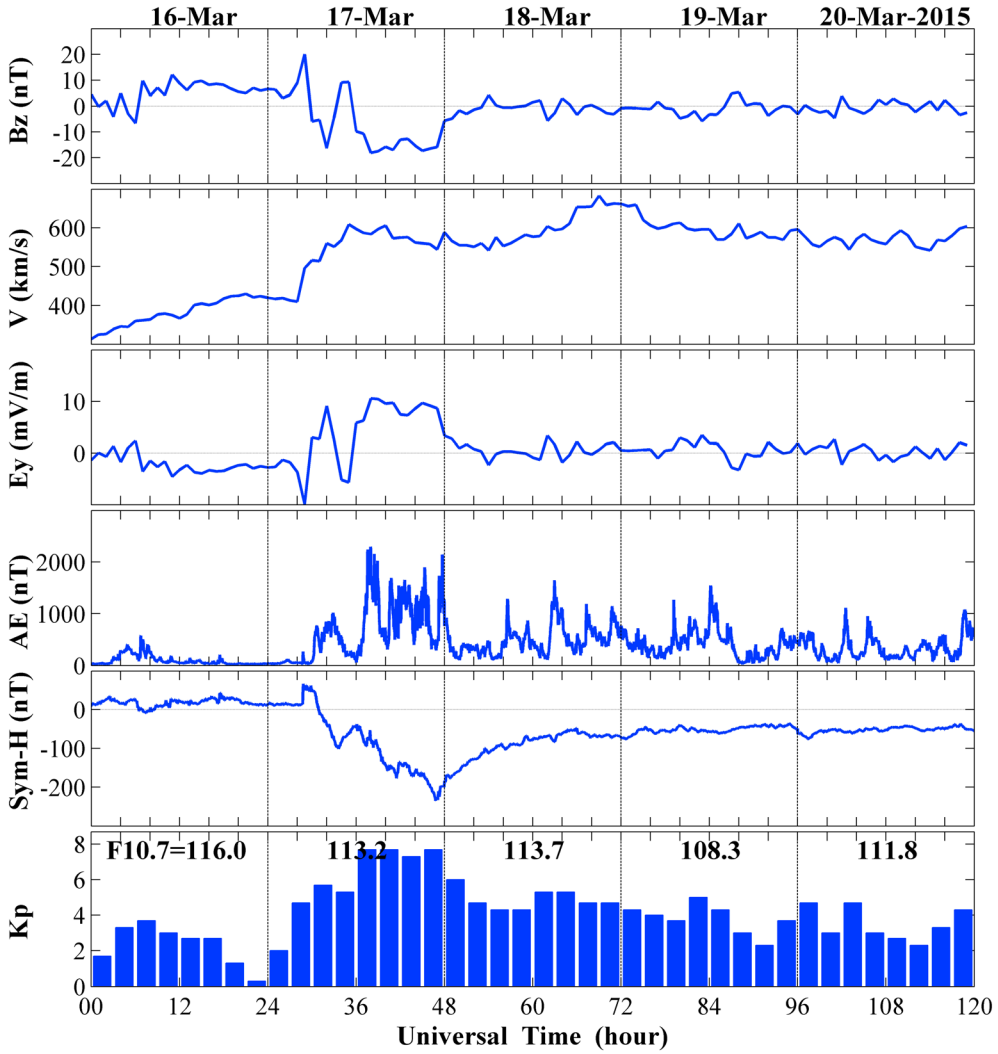

Figure 1. The interplanetary magnetic field (IMF) B_z component (nT), solar wind speed V (km/s), interplanetary electric field (IEF) E_y component (mV/m), *AE* index (nT), *SYM-H* index (nT), and *Kp* index during 16–20 March 2015.

On 16 March, the day prior to the storm onset, TECs have a positive phase in the equatorial ionization anomaly (EIA) region from 12:00 UT to 24:00 UT. This prestorm enhancements in TEC at low latitude over the Asian-Australian sector are consistent with the features reported by *Liu et al.* [2008]. They suggested that the zonal electric fields are the more likely causes to create the low-latitude prestorm enhancements. As seen from Figure 2 (middle), DTEC presents a salient positive phase in the daytime EIA regions and a negative phase in the same regions on the nighttime on 17 March. Especially, the EIA is significantly suppressed and the intensive negative storm effects in the regions of two crests last from the daytime to the nighttime on 18 March. Similar to 17 March, TEC presents a positive storm effect on the daytime and an inconspicuous negative storm effect on the nighttime in the EIA regions with a weaker magnitude on 19 March. On 17 March, $\Delta H_{\text{cdo-mut}}$ has an increase to ~70 nT after 06:00 UT as a consequence of the sudden southward turning of IMF B_z (seen in Figure 1) due to the undershielding effect, producing eastward PEFs on the dayside. After that, the equatorial electrojet has undergone multiple oscillations showing similar variations as the IMF B_z until ~09:30 UT. It seems that the enhanced eastward PEFs have played a significant role in the TEC enhancement in the daytime EIA regions on 17 March. The equatorial electrojet has a westward reversal with a weak magnitude about −20 nT from 10:00 UT to 12:00 UT on 17 March. It coincides with the northward turning of IMF B_z, which could produce westward PEFs due to the overshielding effect. During the daytime of 18 March, $\Delta H_{\text{cdo-mut}}$ has a salient negative phase to a minimum of −65 nT and this westward equatorial electrojet lasts

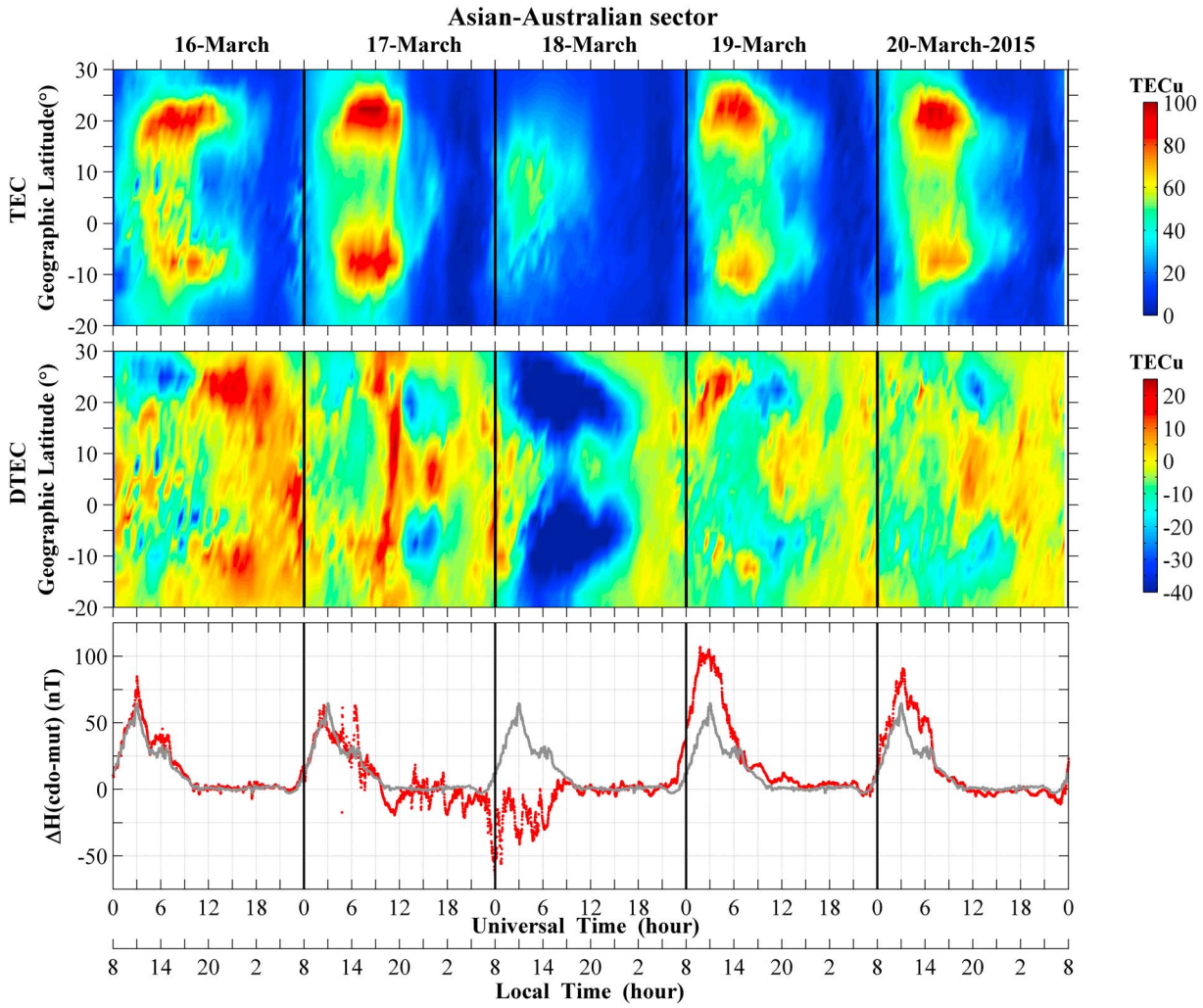

Figure 2. (top) The TEC and (middle) the deviations of TEC (DTEC) at longitude ~120°E and (bottom) the variations of $\Delta H_{\text{cdo-mut}}$ on 16–20 March 2015. The gray curve in Figure 2 (bottom) denotes the reference values, derived from the mean values of $\Delta H_{\text{cdo-mut}}$ on 15–16 March. The mean TEC data of five international quiet days of the month are used as the reference values to obtain the DTEC.

for almost the entire daytime. Taking the interplanetary condition into account, the direction and the duration, the most likely electric fields here are DDEFs, which are typically westward on the dayside and occur often with a long duration [*Blanc and Richmond*, 1980; *Bagiya et al.*, 2011]. The strong westward DDEFs may strongly suppress the generation of the EIA on the daytime of 18 March. In the next day (19 March), the enhanced daytime eastward ionospheric electric fields could make the TEC enhancement in the daytime EIA regions, which are similar to the daytime of 17 March, but the positive storm effects on the day are weaker. Particularly, the enhanced daytime eastward ionospheric fields are probably derived from the day-to-day variability of the ionosphere according to the condition of IMF B_z and the inconsistent direction with the normal westward DDEF on the dayside.

In order to explore more storm time ionospheric features, especially for the nighttime, the ionospheric parameters at two stations at low latitudes over this sector are utilized. Figure 3 gives the variations of foF_2 and h_mF_2 at Sanya and Guam on 16–20 March 2015. The gray curves denote the mean values of five international quiet days of the month. The top schematic diagram displays the geographic positions of the two stations, and the black curve in the diagram is the position of dip equator. The gray bars indicate the period within 18:00–06:00 LT for each station. Compared with the DTEC in Figure 2, the negative storm effects in Figure 3 are highlighted during these days because of the geographic latitudes of the two stations. During the daytime of 18 March, the negative storm effects at Sanya are also very notable, and the values of h_mF_2

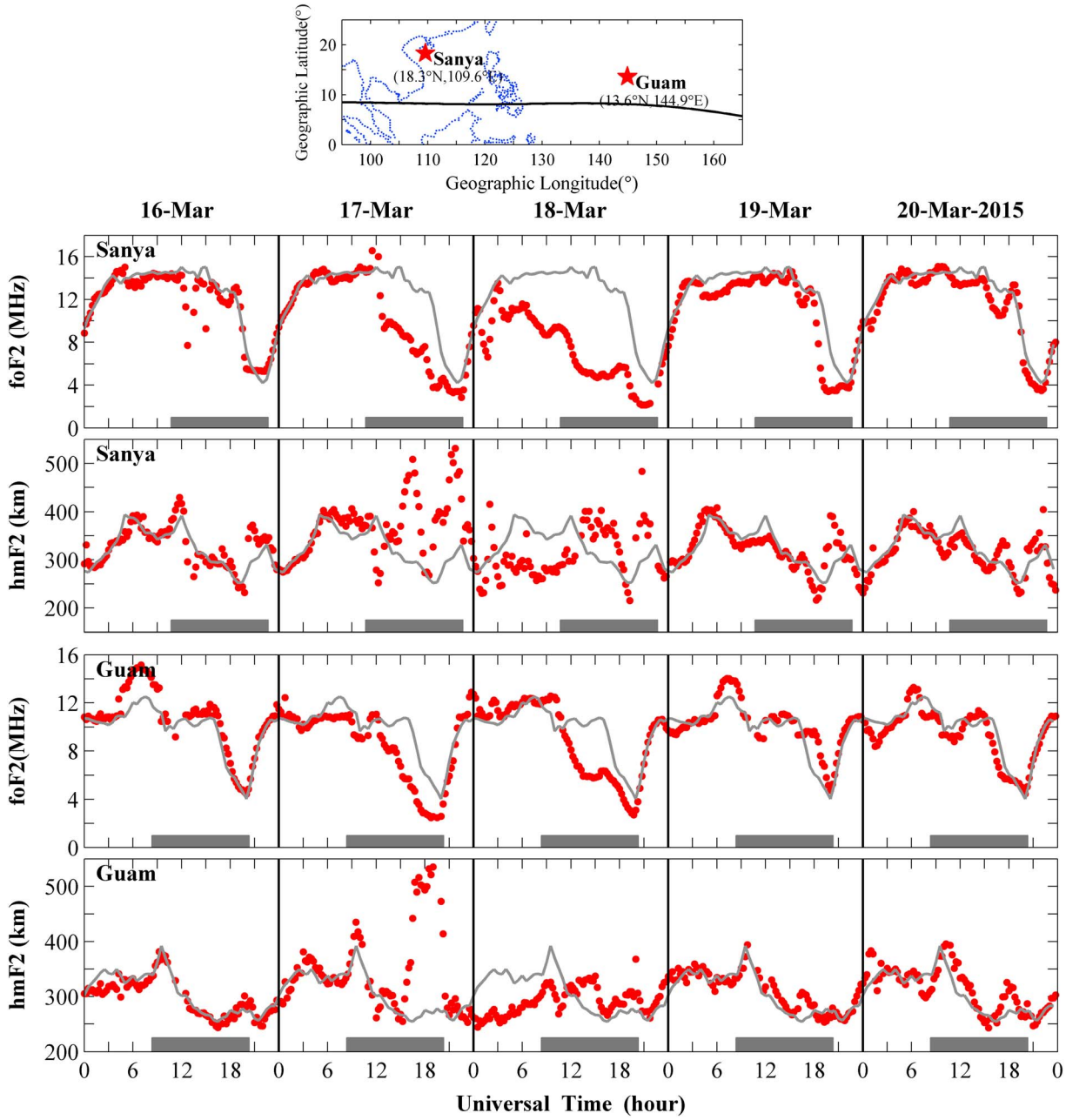

Figure 3. The variations of f_oF_2 and h_mF_2 at Sanya and Guam on 16–20 March 2015. The gray curves denote the mean of five international quiet days of the month. The top schematic diagram displays the geographic positions of the two stations, and the black curve in the diagram shows the position of dip equator. The gray bars indicate the period within 18:00–06:00 LT for each station.

at the two stations drop significantly, which are consistent with the effects of westward DDEFs. Under the action of $\mathbf{E}\times\mathbf{B}$ vertical drift, the westward DDEFs would make the F_2 layer move downward. Moreover, the h_mF_2 at the two East Asian stations have a decline at ~12:00 UT on 17 March, which are probably caused by the westward PEFs over the Asian-Australian sector on the day.

Furthermore, the nighttime negative storm effects at the two stations are more prominent. The intense negative storm effects occur during the nighttime on 17–18 March over Sanya and Guam. Meanwhile, the h_mF_2 have significant enhancements on the two stations. The uplifting effects are most likely caused by the eastward DDEF because of the long duration and the eastward direction at night. We can find that the effects of DDEFs last for about 1.5 days from the nighttime of 17 March to the whole day of 18 March over

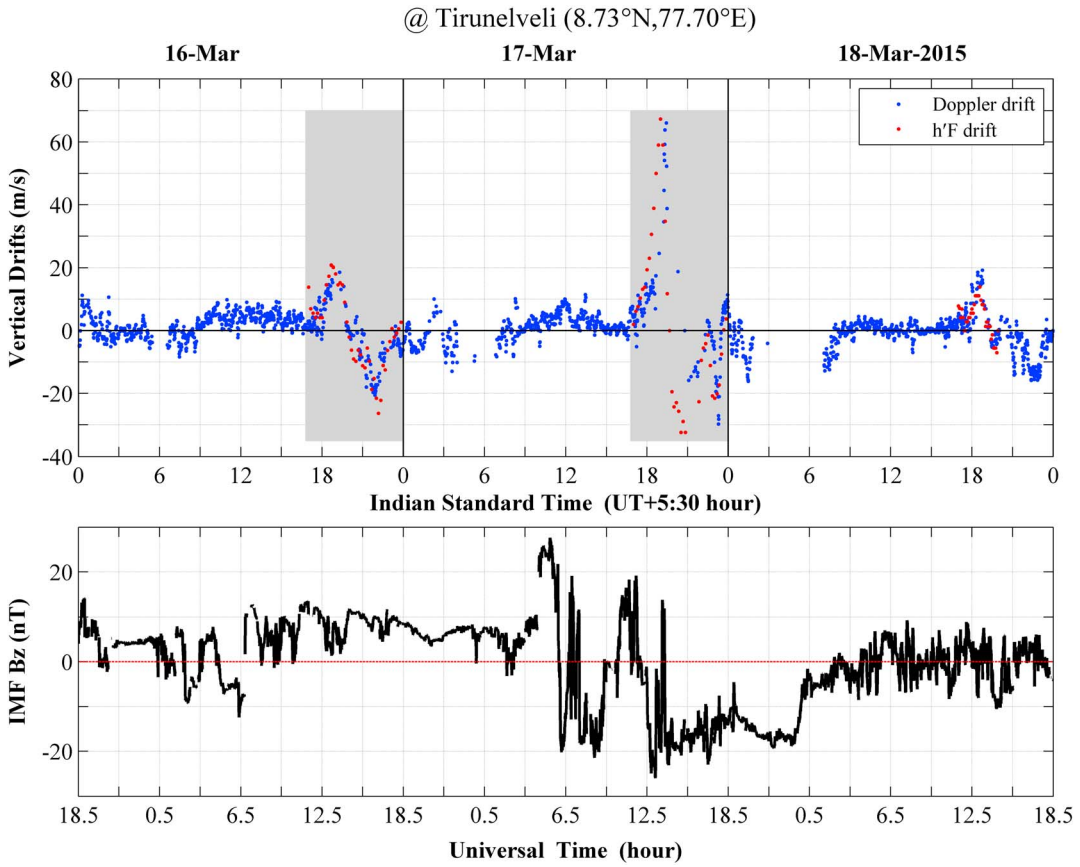

Figure 4. (top) The vertical Doppler drifts (in blue curve) and the vertical drifts obtained from the rate of change of virtual height h'F (in red curve) over an equatorial station Tirunelveli on 16–18 March 2015. (bottom) The variations of IMF B_z are also displayed. The drifts on 16 March are used as the quiet time reference values.

the Asian-Australian sector. In addition, some weak nighttime negative storm effects occur at Sanya on 19–20 March and at Guam on 20 March, which are also accompanied with the enhanced h_mF_2. The inconspicuous enhancements are also most likely caused by eastward DDEFs because of the interplanetary condition at night. It seems that the eastward electric fields have played a significant role in the nighttime negative storm effects during the storm time over the two stations. The upward vertical drifts caused by the eastward electric fields may strengthen the transport processes of electrodynamics and accelerate the loss of the plasma to create the negative storm effects during the nighttime in low latitude and equatorial regions. *Liu et al.* [2013] investigated the ionospheric nighttime enhancement (in electron density/ f_oF_2) events over Sanya, getting the conclusion that the westward electric field-induced vertical drifts are essential in forming the nighttime enhancements in f_oF_2 over Sanya. Compared with the nighttime enhancements, it is a reversal process in this case.

Drift data over Indian sector are also analyzed here for comparison. Figure 4 displays the vertical Doppler drifts (top, in blue curve) from the observations of Doppler drift mode and the vertical drifts obtained from the rate of change of virtual height *h'F* (top, in red curve) over an equatorial station Tirunelveli on 16–18 March 2015. The variations of IMF B_z are also plotted in Figure 4 (bottom). The Doppler vertical drifts that we presented in this paper are obtained from 7 MHz frequency because of the better trend and continuity. It is noted that the daytime Doppler drifts come from the effect of the photoionization, which is supported by the lack of the sufficient irregularities [*Ramsingh et al.*, 2015]. The evening time *h'F* drifts are used to substantiate, and the gray shaded area indicates the period of the disturbed vertical drifts. The ion drifts on 16 March can be used as the quiet time reference values. However, strong vertical drift fluctuations occur during the daytime on 17 March and the vertical drifts go up to ~70 m/s at 13:30 UT. It is probably caused by the eastward PEFs according to the sudden southward turning of IMF B_z (seen in Figure 4, bottom) on the

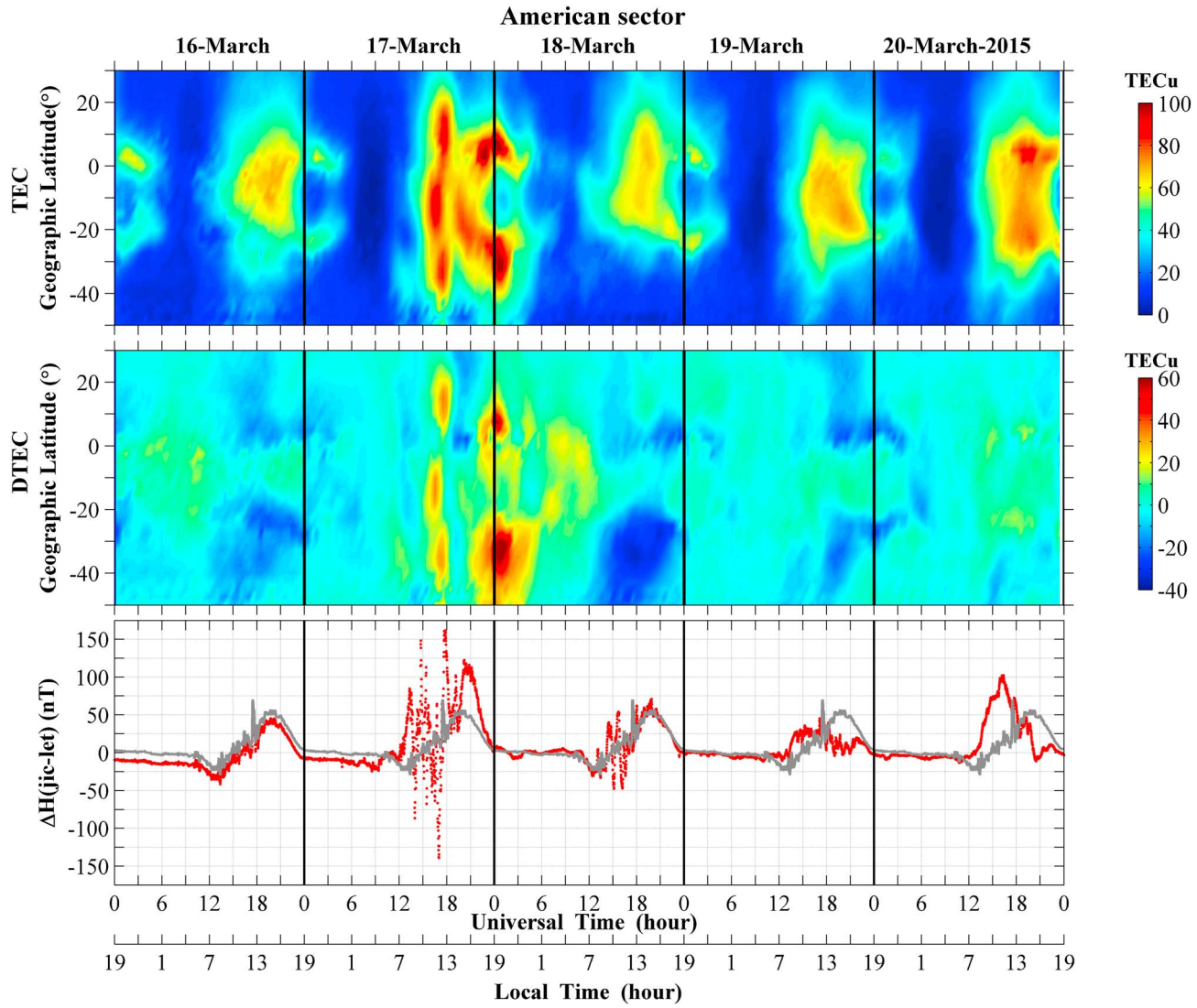

Figure 5. (top) The TEC and (middle) the deviations of TEC (DTEC) at longitude ~70°W and (bottom) the variations of $\Delta H_{\text{jic-let}}$ on 16–20 March 2015. The gray curve in Figure 5 (bottom) denotes the quiet time reference values derived from the $\Delta H_{\text{jic-let}}$ on 16 March. The mean TEC data of five international quiet days of the month are used as the reference values to obtain the DTEC.

dayside. *Ramsingh et al.* [2015] also reported the existence of strong disturbance dynamo during the night on 17 March over Indian sector. These features reflect the similarity with the Asian-Australian sector.

3.3. Low-Latitude Ionospheric Response in the American Sector

Similar to Figure 2, Figure 5 demonstrates the storm time universal time (UT) geographic latitude distributions of TEC (Figure 5, top) and the deviations of TEC (DTEC;Figure 5, middle) in the longitude ~70°W and the variations of $\Delta H_{\text{jic-let}}$ (Figure 5, bottom) on 16–20 March 2015. The gray curve in Figure 5 (bottom) denotes the quiet time reference values derived from the $\Delta H_{\text{jic-let}}$ on 16 March. The mean TEC data of five international quiet days of the month are also used as the reference values to obtain the DTEC. On 16 March, the day prior to the storm onset, TECs have no significant change with the geomagnetically quiet days.

As shown from Figure 5 (middle), the most remarkable feature of DTEC is two consecutive positive storms in the region of equatorial ionization anomaly (EIA) on the daytime of 17 March. Apart from this remarkable feature, a positive phase occurs in the equatorial region during the nighttime (before ~13:00 UT) on 18 March,

and a negative storm event can be seen from 20°S to 50°S (over the entire south EIA crest region) during the daytime on the day. On the last day, 20 March, TECs present an inconspicuous positive phase from ~13:00 UT to ~20:00 UT near the daytime EIA region. As shown from the curve of $\Delta H_{\text{jic-let}}$, the multiple penetrations are the most striking phenomenon during the daytime of 17 March. The multiple penetrations are mostly caused by the eastward PEFs as a consequence of the southward turning of IMF B_z (seen in Figure 1) due to the undershielding effect, where the eastward PEFs map to low latitudes on the dayside. The multiple eastward PEFs may play the decisive role in the two consecutive positive storms over the daytime EIA region on 17 March. The multiple enhanced eastward PEFs strengthen the fountain effects and cause the TEC storm time features. For the next day, 18 March, similar features of the $\Delta H_{\text{jic-let}}$ with a weaker magnitude can be found from ~14:00 UT to ~16:30 UT, which are also caused by the short-lived southward turning of IMF B_z (seen in Figure 1) during that time. On 19–20 March, the main features of the disturbed electric fields are both the enhanced eastward electric fields followed by the reversed westward electric fields during the daytime for the 2 days. The enhanced eastward electric fields may cause the positive phase during the daytime on 20 March.

Similarly, the ionospheric parameters at three stations near the magnetic equator over the American sector are also shown in Figure 6. Figure 6 depicts the variations of f_oF_2 and h_mF_2 at Jicamarca, Sao Luis, and Fortaleza on 16–20 March 2015. The gray curves denote the mean values of five international quiet days of the month. The top schematic diagram displays the geographic positions of the three stations, and the black curve in the diagram gives the position of dip equator. The gray bars indicate the period within 18:00–06:00 LT for each station. The repeated significant uplifts of F_2 layer caused by the multiple eastward PEFs, which can be seen in the curves of h_mF_2 over the three stations from ~12:00 UT to ~24:00 UT on the daytime of 17 March, are also the most salient feature on the American sector during this storm. At the same time, the values of f_oF_2 are in antiphase with h_mF_2 in accompany of the eastward PEFs over the three stations. In the equatorial region, the uplifting effect to the F region caused by the eastward PEFs under the action of $\mathbf{E}\times\mathbf{B}$ vertical drift makes the plasma upward to a higher altitude. Meanwhile, more plasma will diffuse into low latitudes along the magnetic field lines under the combined effects of the gravity and the pressure gradient force, and finally cause the negative ionospheric storm effects in the equatorial regions and the positive ionospheric storm effects in low latitudes. It is consistent with the positive ionospheric storm effects of TEC in the low latitude on 17 March in Figure 5. *Kuai et al.* [2015] reported the antiprocess which causes the daytime positive storms over Jicamarca. This process is also similar with the results reported by *Basu et al.* [2009] and *Liu et al.* [2012], in which daytime EIA structure collapses under the function of reversal electrojet and electron density enhancements over the EIA trough region.

Another noteworthy feature is the significant elevation of h_mF_2 for more than 150 km from ~03:00 UT to ~12:00 UT on the nighttime of 18 March. The uplifting effects are most likely caused by eastward DDEF because of the long duration and the eastward direction at the nightside. Accompanied with the significant elevation of h_mF_2, the values of f_oF_2 have a positive phase during the nighttime on 18 March. It seems that the effect of the recombination process is relatively important because of the low recombination rates at higher altitudes. Besides these main features, some positive phases in f_oF_2 with weak declines in h_mF_2 can be seen during the daytime on 18–20 March. By the way, the previously mentioned negative storm event from 20°S to 50°S during the daytime on 18 March should be caused by other physical mechanisms apart from the disturbed electric fields, because no suitable disturbed electric fields can be responsible for this negative storm effect. *Astafyeva et al.* [2015] analyzed the thermospheric [O]/[N_2] ratios as measured by the Global Ultraviolet Imager satellite on 17–18 March 2015 in the local morning sector (~10:00 LT). According to the result, the [O]/[N_2] ratio on 18 March is lower than it on 17 March with a magnitude great than 0.3 at ~15:00 UT over this region. Ionospheric F layer electron production is determined by the photoionization of atomic O, while the recombination is under the control of the density of molecular gases (N_2 and O_2). So the electron density is proportional to the ratio [O]/[N_2] when the transport process is less relatively important. It is possible to infer that the composition changes would play an important role in this negative storm effect on 18 March over this region. *Fagundes et al.* [2016] also found a strong positive phase under the action of an eastward PEF during the main phase of the March 2015 storm and a negative storm caused by [O]/[N_2] ratio changes during the recovery phase over the Brazilian sector, which are similar with the feature over the American sector.

As a supplementary evidence to the multiple PEFs, the phenomenon of the storm time F_3 layer is very obvious at the three stations over the American sector on 17 March. Many researchers have investigated

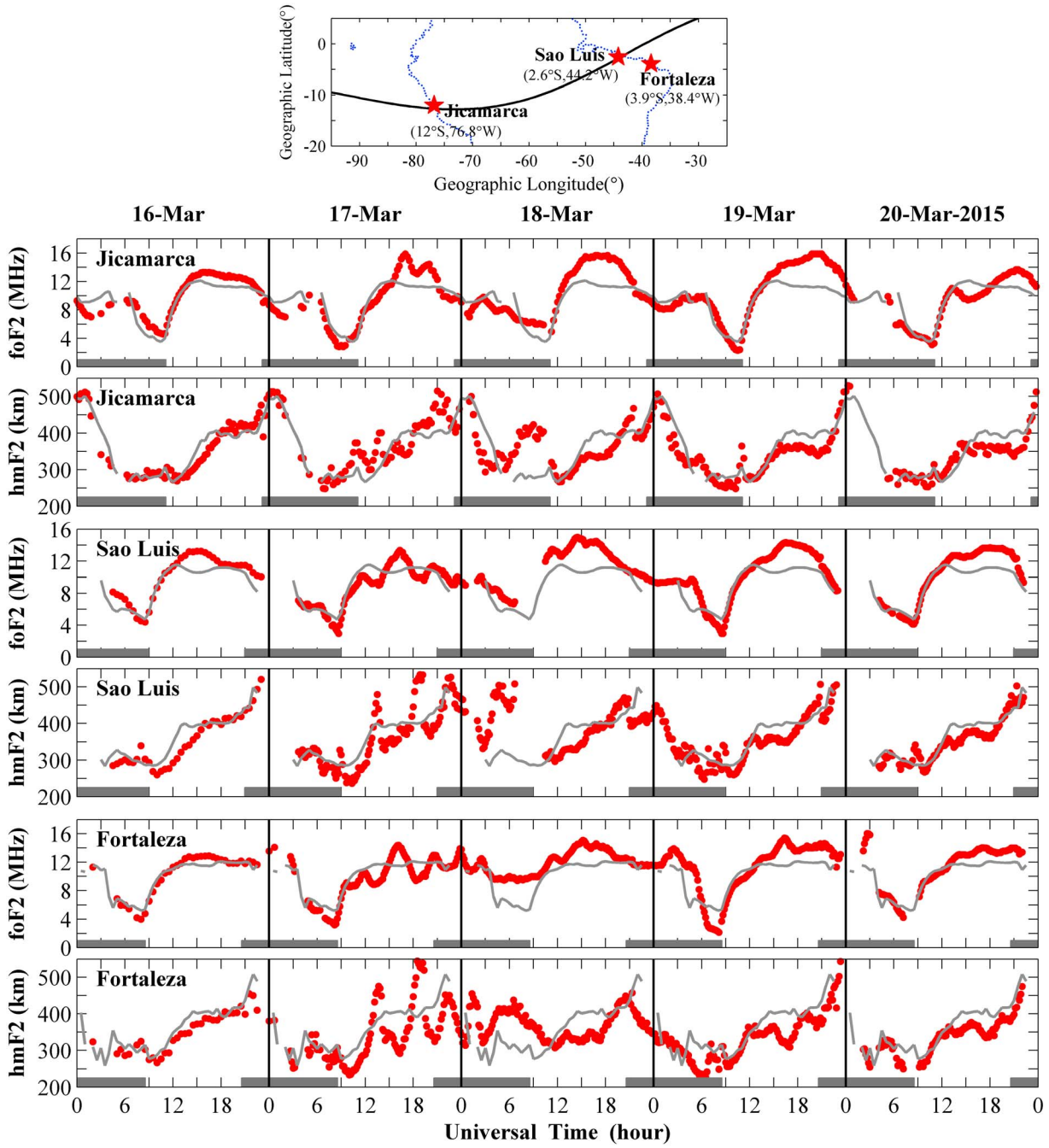

Figure 6. The variations of f_oF_2 and h_mF_2 at Jicamarca, Sao Luis, and Fortaleza on 16–20 March 2015. The gray curves denote the mean of five international quiet days of the month. The top schematic diagram displays the geographic positions of the three stations, and the black curve in the diagram gives the position of dip equator. The gray bars indicate the period within 18:00–06:00 LT for each station.

the features of the F_3 layer during the geomagnetically quiet conditions and the geomagnetic storms [e.g., *Balan et al.*, 1997, 1998, 2008; *Jenkins et al.*, 1997; *Hsiao et al.*, 2001; *Zhao et al.*, 2005, 2011, 2014; *Zain et al.*, 2008; *Lin et al.*, 2009a, 2009b; *Sreeja et al.*, 2009, 2010; *Klimenko et al.*, 2011; *Zhang et al.*, 2016].

Figure 7 exhibits the ionograms caught by the SAO-Explorer software over (a) Jicamarca, (b) Sao Luis, and (c) Fortaleza on 17 March 2015. Two images are caught for every station, and the corresponding time is marked on each image. During this geomagnetic storm, two periods of this F_3 layer phenomenon are found for each station, which are consistent with the time of the significant elevations of h_mF_2 (seen in Figure 6) caused by

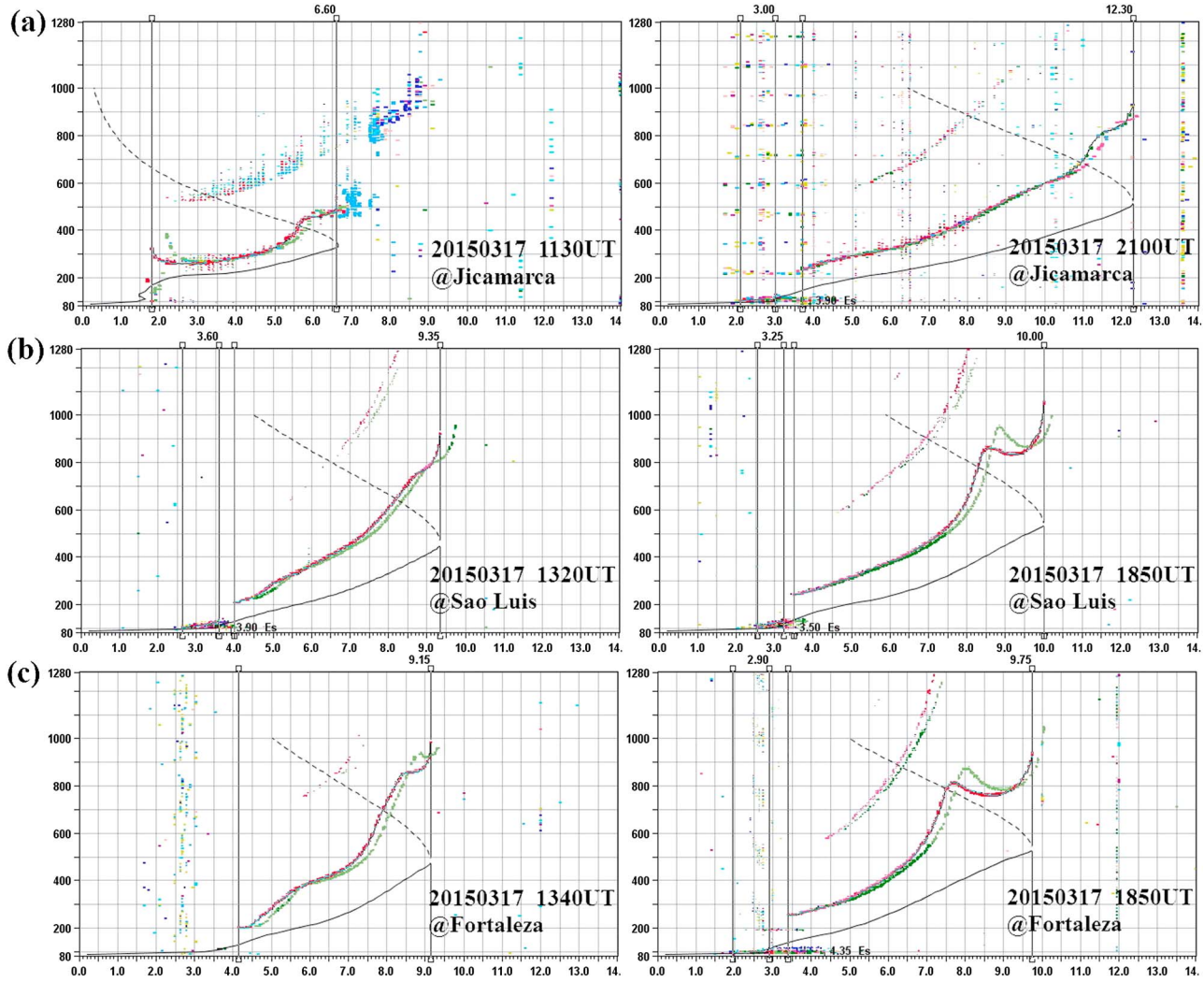

Figure 7. The ionograms at two times over (a) Jicamarca, (b) Sao Luis, and (c) Fortaleza on 17 March 2015.

the multiple eastward PEFs. Therefore, Figure 7 shows one ionogram image for each period of the storm time F_3 layer in the three stations. The mechanism of this storm time F_3 layer is probably caused by the rapid upward $\mathbf{E}\times\mathbf{B}$ drifts resulting from the multiple eastward PEFs, and the intensification of the F_3 layer over Sao Luis and Fortaleza at ~18:30 UT also reflects the strong magnetospheric prompt penetration electric fields [*Zhao et al.*, 2005; *Paznukhov et al.*, 2007; *Balan et al.*, 2008; *Lin et al.*, 2009a; *Sreeja et al.*, 2009; *Klimenko et al.*, 2011]. To demonstrate this process, Figure 8 displays the ionograms from 18:00 UT to 19:20 UT over Sao Luis on 17 March 2015. The time series of these ionograms from 18:00 UT to 19:10 UT clearly show the complete process that the storm time F_3 layer is gradually uplifted under the effects of the strong PEFs. Seen from the last ionogram in Figure 8, the storm time F_3 layer vanishes and the h_mF_2 drops to a relatively low value at 19:20 UT. In addition, the storm time F_3 layer is not observed in the two East Asian stations during this event, which is different with the phenomenon in the American equatorial region. *Ramsingh et al.* [2015] reported that the storm time F_3 layer also occurs at Tirunelveli over Indian sector. More analyses are required to obtain the reason for the differences over these sectors.

3.4. Differences in the Characteristics of the Disturbed Electric Fields

During geomagnetic storm events, the penetration electric field (PEF) responses to prompt penetration of convection electric fields and disturbance dynamo electric field (DDEF) generated by the disturbance

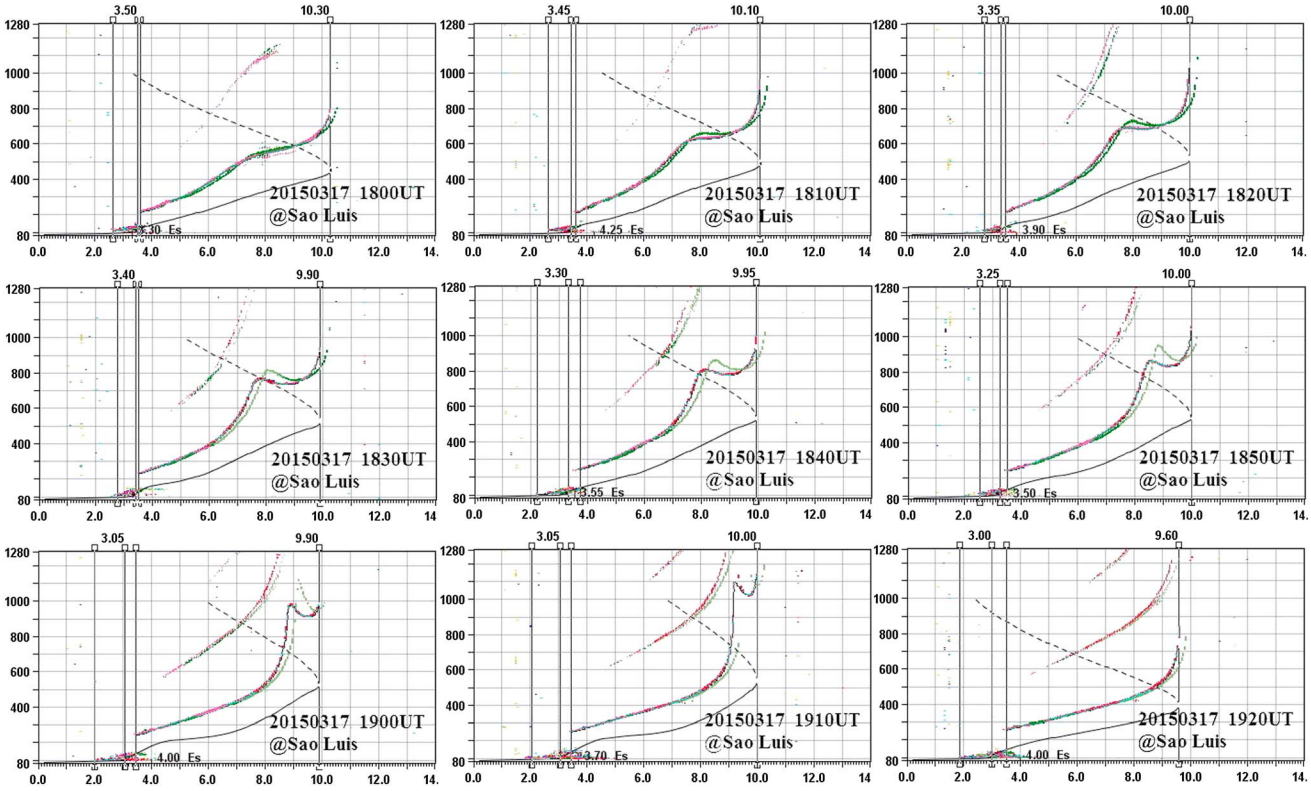

Figure 8. The ionograms from 18:00 UT to 19:20 UT over Sao Luis on 17 March 2015.

dynamo effectively influence the development of the positive and negative storm effects [e.g., *Prölss*, 1995; *Lu et al.*, 2001; *Shreedevi et al.*, 2016]. Especially over the equatorial region, the ionospheric storm effects respond to both the disturbed electric fields during the entire process of geomagnetic storms [*Sobral et al.*, 2001; *Kuai et al.*, 2015]. The role of the composition changes and thermodynamics would be weakened in low latitude and equatorial regions [*Buonsanto*, 1999, references therein]. Our investigations show similar features during this intense storm. It is obvious that the disturbed electric fields play a decisive role in the ionospheric storm effects in low latitude and equatorial regions in both the Asian-Australian sector and the American sector during this event. The eastward PEFs occur in both the Asian-Australian sector and the American sector on 17 March, which is an unusual phenomenon for this geomagnetic storm. Similarly, the DDEFs play an important role in the ionospheric response in both the two sectors during this event. *Nava et al.* [2016] separated the PEFs and the DDEFs on the basis of magnetometer data using the spectral analysis during the March 2015 storm, which is in agreement with our results. Besides these commonalities, the differences of the characteristics also exist. For comparison, Figure 9 plots the variations of (a) IMF B_z; (b and c) h_mF_2 at Sanya and Guam; (d) $\Delta H_{\text{jic-let}}$; (e–g) h_mF_2 at Jicamarca, Sao Luis, and Fortaleza; and (*h*) the vertical Doppler drifts at Tirunelveli during 12:00–24–00 UT of 17 March. The gray curves of Figures 9b–9h denote the quiet time reference values of these parameters. The gray shaded areas indicate the period within 18:00–06:00 LT for each station. As shown in Figure 9a, the southward IMF B_z lasts for about 12 h during the main phase of the great storm. The twice long-term eastward PEFs occur in the daytime sector over the American region during this period (Figures 9d–9g). The first long-term PEF occurs during 13:00–15:00 UT, which drives obvious ionosphere upward movement in the American sector but very small changes in the East Asian area. As shown in Figure 9, the h_mF_2 in the three American stations have the significant elevations of ~100 km during 13:00–15:00 UT (Figures 9e–9g), which the h_mF_2 in the two Asian stations have no remarkable elevation. In addition, the eastward PEF can also be found at sunset during 13:00–15:00 UT over the Indian sector (Figure 9h). *Tulasi Ram et al.* [2016] also reported the unusually enhanced equatorial zonal electric field in response to the PEF on sunset terminator over the Indian sector. All these features indicate the strong local time dependence of PEFs. For the second time, strong ionosphere upward lifts occur in both the American and Asian-Australian sector during 18:00–20:00 UT when

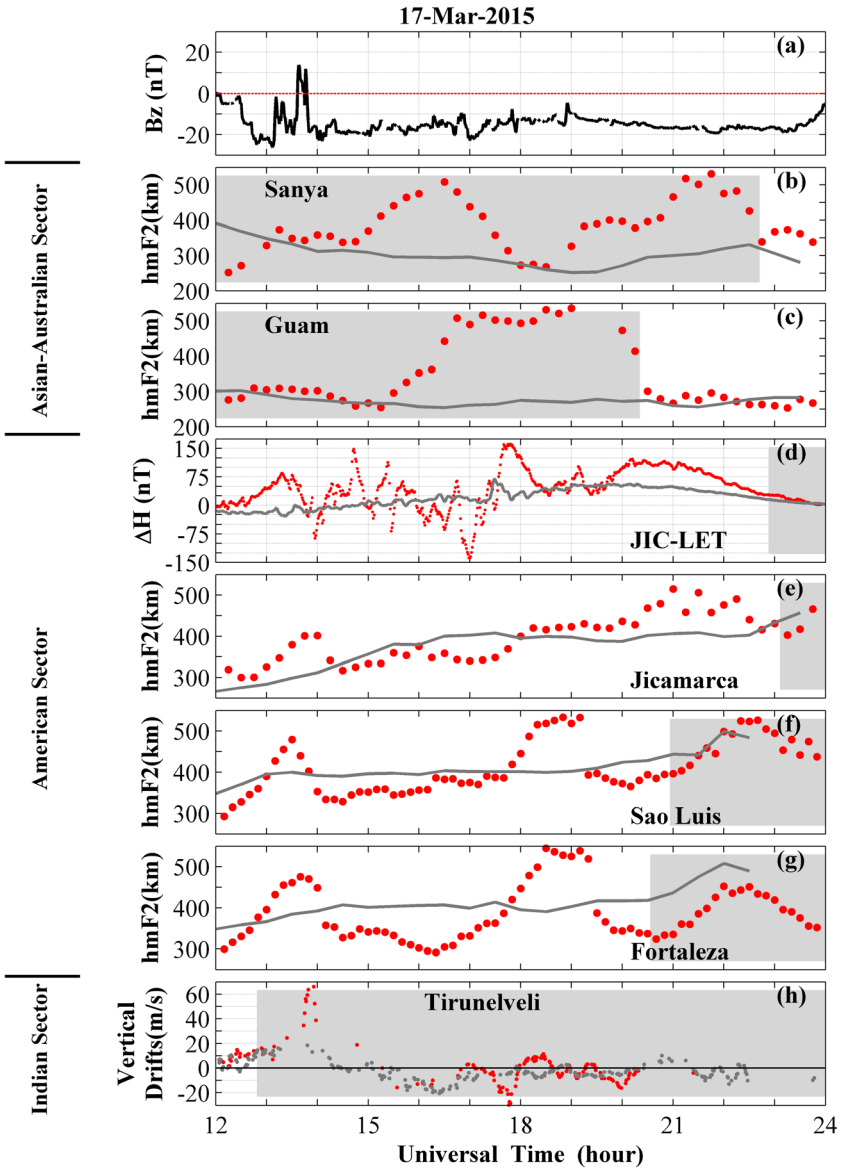

Figure 9. The variations of (a) IMF B_z; (b and c) h_mF_2 at Sanya and Guam; (d) $\Delta H_{\text{jic-let}}$; (e–g) h_mF_2 at Jicamarca, Sao Luis, and Fortaleza; and (h) the vertical Doppler drifts at Tirunelveli during 12:00–24:00 UT of 17 March. The gray curves of Figures 9b–9h denote the quiet time reference values of these parameters. The gray shaded areas indicate the period within 18:00–06:00 LT for each station.

the IMF B_z has a relative steady value. Currently, we do not have solid explanation for this phenomenon. It could be related to the combined effects of PEFs and DDEFs. Due to the strong local time dependence of the disturbance electric fields [e.g., *Fejer et al.*, 1979, 1983, 2008; *Fejer*, 1986, 2002; *Fejer and Scherliess*, 1995, 1997, 1998; *Scherliess and Fejer*, 1997; *Huang*, 2013], DDEFs are eastward in the postmidnight sector, which cannot be balanced by westward PEF, producing remarkable upward drifts in the East Asian sector. In the American equatorial ionosphere, the daytime upward movement is mostly related to eastward PEF, which dominates over DDEF. It is clear that both the PEFs and DDEFs show the notable local time dependence, which makes the sector differences in the characteristics of the disturbed electric fields. Finally, the differences in the characteristics and strength of the disturbed electric fields would directly lead to the sector differences in the low-latitude ionospheric response during the great geomagnetic storm. Overall, the repeated elevations of h_mF_2 by the multiple PEFs are distinctive over the American sector, while the strong negative storm effects caused by the DDEFs are

more notable over the Asian-Australian sector during the March 2015 storm. It should be noted that these characteristics are only derived from this event; more statistical analyses are required to obtain the ionospheric storm effects in different sectors and the sector differences in the ionospheric response during space weather events [e.g., *Thomas et al.*, 2016; *Upadhayaya et al.*, 2016].

4. Conclusions

In this work, we investigated the profound ionospheric disturbances in low latitude and equatorial regions during the March 2015 geomagnetic storm, which is an extremely event with the minimum *SYM-H* value −233 nT in the current 24th solar cycle. The decisive roles of the disturbed electric fields, which comprise penetration electric fields (PEFs) and disturbance dynamo electric fields (DDEFs), are emphasized in low latitude and equatorial regions in both the Asian-Australian sector and the American sector during this event. The major conclusions are summarized as follows:

1. In the Asian-Australian sector, the PEFs occur on the daytime of 17 March. The negative storm effects caused by the westward DDEFs on the daytime of 18 March and the eastward DDEFs on the nighttime of 17–18 March are the main features over this sector during the March 2015 storm. The effects of DDEFs last for about 1.5 days from the nighttime of 17 March to the whole day of 18 March over the Asian-Australian sector. The PEFs are also found over the Indian sector on 17 March. A prominent prestorm enhancement in DTEC is primarily observed on 16 March in low latitude and equatorial regions over the Asian-Australian sector.
2. For the American sector, the multiple strong eastward PEFs and the repeated significant elevations of h_mF_2 on the daytime of 17 March are the most salient feature during the storm. The eastward DDEFs also occur on the nighttime of 18 March, causing the positive storm effects in the equatorial ionosphere over the American sector.
3. The recurrent storm time F_3 layer features are observed in the equatorial region over the American sector on 17 March, proving the effects of the rapid upward $\mathbf{E}\times\mathbf{B}$ drifts resulting from the multiple strong eastward PEFs.
4. The disturbed electric fields play a decisive role in the ionospheric storm effects in low latitude and equatorial regions in both the Asian-Australian sector and the American sector during this event.
5. Both the DDEFs and PEFs show the notable local time dependence, which makes the sector differences in the characteristics of the disturbed electric fields. The differences in the characteristics and strength of the disturbed electric fields would directly lead to the sector differences in the low-latitude ionospheric response during the great geomagnetic storm. Overall, the ionospheric disturbances and the repeated elevations of h_mF_2 caused by the multiple strong PEFs are distinctive over the American sector, while the negative storm effects caused by the long-duration DDEFs are more striking over the Asian-Australian sector during the March 2015 storm.

Acknowledgments
The OMNI data are downloaded from the OMNIWeb interface at http://omniweb.gsfc.nasa.gov. Thanks to B.W. Reinisch from the Center for Atmospheric Research, University of Massachusetts Lowell, for providing the ionogram data of DIDBase. GPS TECs are provided by the MIT Haystack Observatory Madrigal database (http://www.openmadrigal.org). The data of drifts over Indian sector are provided by S. Sripathi from Indian Institute of Geomagnetism. The data of IQDs are obtained from the website of Geoscience Australia (http://www.ga.gov.au/oracle/geomag/iqd_form.jsp). This research is supported by the National Natural Science Foundation of China (41231065, 41321003, and 41304128), the Chinese Academy of Sciences project (KZZD-EW-01-3), and the National Key Basic Research Program of China (2012CB825604). We acknowledge the use of data from the Chinese Meridian Project.

References

Abdu, M. A. (1997), Major phenomena of the equatorial ionosphere thermosphere system under disturbed conditions, *J. Atmos. Sol. Terr. Phys.*, *59*, 1505–1519, doi:10.1016/S1364-6826(96)00152-6.

Anderson, D., A. Anghel, K. Yumoto, M. Ishitsuka, and E. Kudeki (2002), Estimating daytime vertical E × B drift velocities in the equatorial F-region using ground-based magnetometer observations, *Geophys. Res. Lett.*, *29*(12), 1596, doi:10.1029/2001GL014562.

Astafyeva, E., I. Zakharenkova, and M. Förster (2015), Ionospheric response to the 2015 St. Patrick's Day storm: A global multi-instrumental overview, *J. Geophys. Res. Space Physics*, *120*, 9023–9037, doi:10.1002/2015JA021629.

Bagiya, M. S., K. N. Iyer, H. P. Joshi, S. V. Thampi, T. Tsugawa, S. Ravindran, R. Sridharan, and B. M. Pathan (2011), Low-latitude ionospheric-thermospheric response to storm time electrodynamical coupling between high and low latitudes, *J. Geophys. Res.*, *116*, A01303, doi:10.1029/2010JA015845.

Balan, N., G. J. Bailey, M. A. Abdu, K. I. Oyama, P. G. Richards, J. Macdougall, and I. S. Batista (1997), Equatorial plasma fountain and its effects over three locations: Evidence for an additional layer, the F3 layer, *J. Geophys. Res.*, *102*, 2047–2056, doi:10.1029/95JA02639.

Balan, N., I. S. Batista, M. A. Abdu, J. Macdougall, and G. J. Bailey (1998), Physical mechanism and statistics of occurrence of an additional layer in the equatorial ionosphere, *J. Geophys. Res.*, *103*, 29,169–29,181, doi:10.1029/98JA02823.

Balan, N., S. V. Thampi, K. Lynn, Y. Otsuka, H. Alleyne, S. Watanabe, M. A. Abdu, and B. G. Fejer (2008), F3 layer during penetration electric field, *J. Geophys. Res.*, *113*, A00A07, doi:10.1029/2008JA013206.

Basu, S., S. Basu, J. Huba, J. Krall, S. E. McDonald, J. J. Makela, E. S. Miller, S. Ray, and K. Groves (2009), Day-to-day variability of the equatorial ionization anomaly and scintillations at dusk observed by GUVI and modeling by SAMI3, *J. Geophys. Res.*, *114*, A04302, doi:10.1029/2008JA013899.

Blanc, M., and A. D. Richmond (1980), The ionospheric disturbance dynamo, *J. Geophys. Res.*, *85*, 1669–1686, doi:10.1029/JA085iA04p01669.

Buonsanto, M. J. (1999), Ionospheric storm—A review, *Space Sci. Rev.*, *88*, 563–601, doi:10.1023/A:1005107532631.

Burns, A. G., T. L. Killeen, and R. G. Roble (1989), Processes responsible for the compositional structure of the thermosphere, *J. Geophys. Res.*, *94*, 3670–3686, doi:10.1029/JA094iA04p03670.

Burns, A. G., S. C. Solomon, W. Wang, and T. L. Killeen (2007), The ionospheric and thermospheric response to CMEs: Challenges and successes, *J. Atmos. Sol. Terr. Phys.*, *69*, 77–85, doi:10.1016/j.jastp.2006.06.010.

Carter, B. A., E. Yizengaw, R. Pradipta, J. M. Retterer, K. Groves, C. Valladares, R. Caton, C. Bridgwood, R. Norman, and K. Zhang (2016), Global equatorial plasma bubble occurrence during the 2015 St. Patrick's Day storm, *J. Geophys. Res. Space Physics*, *121*, 894–905, doi:10.1002/2015JA022194.

Danilov, A. D. (2013), Ionospheric F-region response to geomagnetic disturbances, *Adv. Space Res.*, *52*, 343–366, doi:10.1016/j.asr.2013.04.019.

Danilov, A. D., and J. Lăstovička (2001), Effects of geomagnetic storms on the ionosphere and atmosphere, *Int. J. Geomagn. Aero.*, *2*, 209–224.

Fagundes, P. R., F. A. Cardoso, B. G. Fejer, K. Venkatesh, B. A. G. Ribeiro, and V. G. Pillat (2016), Positive and negative GPS-TEC ionospheric storm effects during the extreme space weather event of March 2015 over the Brazilian sector, *J. Geophys. Res. Space Physics*, *121*, 5613–5625, doi:10.1002/2015JA022214.

Fejer, B. G. (1986), Equatorial ionospheric electric fields associated with magnetospheric disturbances, in *Solar Wind Magnetosphere Coupling*, edited by Y. Kamide and J. A. Slavin, pp. 519–545 , Terra Sci., Tokyo.

Fejer, B. G. (1997), The electrodynamics of the low-latitude ionosphere: Recent results and future challenges, *J. Atmos. Sol. Terr. Phys.*, *59*, 1465–1482, doi:10.1016/S1364-6826(96)00149-6.

Fejer, B. G. (2002), Low latitude storm time ionospheric electrodynamics, *J. Atmos. Sol. Terr. Phys.*, *64*, 1401–1408, doi:10.1016/S1364-6826(02)00103-7.

Fejer, B. G. (2011), Low latitude ionospheric electrodynamics, *Space Sci. Rev.*, *158*, 145–166, doi:10.1007/s11214-010-9690-7.

Fejer, B. G., and L. Scherliess (1995), Time dependent response of equatorial ionospheric electric fields to magnetospheric disturbances, *Geophys. Res. Lett.*, *22*, 851–854, doi:10.1029/95GL00390.

Fejer, B. G., and L. Scherliess (1997), Empirical models of storm time equatorial zonal electric fields, *J. Geophys. Res.*, *102*, 24,047–24,056, doi:10.1029/97JA02164.

Fejer, B. G., and L. Scherliess (1998), Mid- and low-latitude prompt ionospheric zonal plasma drifts, *Geophys. Res. Lett.*, *25*, 3071–3074, doi:10.1029/98GL02325.

Fejer, B. G., C. A. Gonzalez, D. T. Farley, and M. C. Kelly (1979), Equatorial electric fields during magnetically disturbed conditions: 1. The effect of the interplanetary magnetic field, *J. Geophys. Res.*, *84*, 5797–5802, doi:10.1029/JA084iA10p05797.

Fejer, B. G., M. F. Larsen, and D. T. Farley (1983), Equatorial disturbance dynamo electric fields, *Geophys. Res. Lett.*, *10*, 537–540, doi:10.1029/GL010i007p00537.

Fejer, B. G., J. W. Jensen, and S.-Y. Su (2008), Seasonal and longitudinal dependence of equatorial disturbance vertical plasma drifts, *Geophys. Res. Lett.*, *35*, L20106, doi:10.1029/2008GL035584.

Fenrich, F. R., and J. G. Luhmann (1998), Geomagnetic response to magnetic clouds of different polarity, *Geophys. Res. Lett.*, *25*, 2999–3002, doi:10.1029/98GL51180.

Habarulema, J. B., Z. T. Katamzi, and E. Yizengaw (2015), First observations of poleward large-scale traveling ionospheric disturbances over the African sector during geomagnetic storm conditions, *J. Geophys. Res. Space Physics*, *120*, 6914–6929, doi:10.1002/2015JA021066.

Hsiao, C. C., J. Y. Liu, R. T. Tsunoda, S. Fukao, S. Saroso, K. Nozaki, V. L. Badillo, F. T. Berkey, S. W. Chen, and M. Yamamoto (2001), Evidence for the geographic control of additional layer formation in the low latitude ionosphere, *Adv. Space Res.*, *27*, 1293–1297, doi:10.1016/S0273-1177(01)00206-X.

Huang, C. M. (2013), Disturbance dynamo electric fields in response to geomagnetic storms occurring at different universal times, *J. Geophys. Res. Space Physics*, *118*, 496–501, doi:10.1029/2012JA018118.

Huang, C.-S., J. C. Foster, and M. C. Kelley (2005), Long-duration penetration of the interplanetary electric field to the low-latitude ionosphere during the main phase of magnetic storms, *J. Geophys. Res.*, *110*, A11309, doi:10.1029/2005JA011202.

Huang, X., and B. W. Reinisch (1996), Vertical electron density profile from the Digisonde network, *Adv. Space Res.*, *18*, 121–129, doi:10.1016/0273-1177(95)00912-4.

Jenkins, B., G. J. Bailey, M. A. Abdu, I. S. Batista, and N. Balan (1997), Observations and model calculations of an additional layer in the topside ionosphere above Fortaleza, Brazil, *Ann. Geophys.*, *15*, 753–759, doi:10.1007/s00585-997-0753-3.

Kataoka, R., D. Shiota, E. Kilpua, and K. Keika (2015), Pileup accident hypothesis of magnetic storm on 17 March 2015, *Geophys. Res. Lett.*, *42*, 5155–5161, doi:10.1002/2015GL064816.

King, J. H., and N. E. Papitashvili (2005), Solar wind spatial scales in and comparisons of hourly Wind and ACE plasma and magnetic field data, *J. Geophys. Res.*, *110*, A02104, doi:10.1029/2004JA010649.

Klimenko, M. V., V. V. Klimenko, K. G. Ratovsky, L. P. Goncharenko, Y. Sahai, P. R. Fagundes, R. de Jesus, A. J. de Abreu, and A. M. Vesnin (2011), Numerical modeling of ionospheric effects in the middle- and low-latitude F region during geomagnetic storm sequence of 9–14 September 2005, *Radio Sci.*, *46*, RS0D03, doi:10.1029/2010RS004590.

Kuai, J., L. Liu, J. Liu, B. Zhao, Y. Chen, H. Le, and W. Wan (2015), The long-duration positive storm effects in the equatorial ionosphere over Jicamarca, *J. Geophys. Res. Space Physics*, *120*, 1311–1324, doi:10.1002/2014JA020552.

Lin, C. H., A. D. Richmond, J. Y. Liu, G. J. Bailey, and B. W. Reinisch (2009a), Theoretical study of new plasma structures in the low-latitude ionosphere during a major magnetic storm, *J. Geophys. Res.*, *114*, A05303, doi:10.1029/2008JA013951.

Lin, C. H., A. D. Richmond, G. J. Bailey, J. Y. Liu, G. Lu, and R. A. Heelis (2009b), Neutral wind effect in producing a storm time ionospheric additional layer in the equatorial ionization anomaly region, *J. Geophys. Res.*, *114*, A09306, doi:10.1029/2009JA014050.

Liu, J., L. Liu, B. Zhao, Y. Wei, L. Hu, and B. Xiong (2012), High-speed stream impacts on the equatorial ionization anomaly region during the deep solar minimum year 2008, *J. Geophys. Res.*, *117*, A10304, doi:10.1029/2012JA018015.

Liu, J., L. Liu, T. Nakamura, B. Zhao, B. Ning, and A. Yoshikawa (2014), A case study of ionospheric storm effects during long-lasting southward IMF Bz-driven geomagnetic storm, *J. Geophys. Res. Space Physics*, *119*, 7716–7731, doi:10.1002/2014JA020273.

Liu, J., W. Wang, A. Burns, X. Yue, S. Zhang, Y. Zhang, and C. Huang (2016), Profiles of ionospheric storm-enhanced density during the 17 March 2015 great storm, *J. Geophys. Res. Space Physics*, *121*, 727–744, doi:10.1002/2015JA021832.

Liu, L., and W. Wan (2016), New understanding achieved from 2 years of Chinese ionospheric investigations, *Sci. Bull.*, *61*(7), 524–542, doi:10.1007/s11434-016-1035-9.

Liu, L., W. Wan, C. C. Lee, B. Ning, and J. Y. Liu (2004), The low latitude ionospheric effects of the April 2000 magnetic storm near the longitude 120°E, *Earth Planets Space*, *56*, 607–612, doi:10.1186/BF03352521.

Liu, L., W. Wan, M.-L. Zhang, B. Zhao, and B. Ning (2008), Prestorm enhancements in NmF2 and total electron content at low latitudes, *J. Geophys. Res.*, *113*, A02311, doi:10.1029/2007JA012832.

Liu, L., Y. Chen, H. Le, B. Ning, W. Wan, J. Liu, and L. Hu (2013), A case study of postmidnight enhancement in F-layer electron density over Sanya of China, *J. Geophys. Res. Space Physics*, *118*, 4640–4648, doi:10.1002/jgra.50422.

Lu, G., A. D. Richmond, R. G. Roble, and B. A. Emery (2001), Coexistence of ionospheric positive and negative storm phases under northern winter conditions: A case study, *J. Geophys. Res.*, *106*, 24,493–24,504, doi:10.1029/2001JA000003.

Mendillo, M. (2006), Storms in the ionosphere: Patterns and processes for total electron content, *Rev. Geophys.*, *44*, RG4001, doi:10.1029/2005RG000193.

Nava, B., J. Rodríguez-Zuluaga, K. AlazoCuartas, A. Kashcheyev, Y. Migoya-Orué, S. M. Radicella, C. Amory-Mazaudier, and R. Fleury (2016), Middle- and low-latitude ionosphere response to 2015 St. Patrick's Day geomagnetic storm, *J. Geophys. Res. Space Physics*, *121*, 3421–3438, doi:10.1002/2015JA022299.

Paznukhov, V. V., B. W. Reinisch, P. Song, X. Huang, T. W. Bullett, and O. Veliz (2007), Formation of an F3 layer in the equatorial ionosphere: A result from strong IMF changes, *J. Atmos. Sol. Terr. Phys.*, *69*, 1292–1304, doi:10.1016/j.jastp.2006.08.019.

Prölss, G. W. (1995), Ionospheric F region storms, in *Handbook of Atmospheric Electrodynamics*, vol. 2, edited by H. Volland, pp. 195–248 , CRC Press, Boca Ration, Fla.

Prölss, G. W. (2008), Ionospheric storms at mid-latitude: A short review, in *Midlatitude Ionospheric Dynamics and Disturbances*, *Geophys. Monogr. Ser.*, vol. 181, edited by P. M. Kintner et al., pp. 9-24, AGU, Washington, D. C., doi:10.1029/181GM03.

Ramsingh, S., S. Sripathi, S. Sreekumar, K. Banola, P. T. Emperumal, and B. S. Kumar (2015), Low-latitude ionosphere response to super geomagnetic storm of 17/18 March 2015: Results from a chain of groundbased observations over Indian sector, *J. Geophys. Res. Space Physics*, *120*, 10,864–10,882, doi:10.1002/2015JA021509.

Rideout, W., and A. Coster (2006), Automated GPS processing for global total electron content data, *GPS Solut.*, *10*, 219–228, doi:10.1007/s10291-006-0029-5.

Sastri, J. H. (1988), Equatorial electric fields of ionospheric disturbance dynamo origin, *Ann. Geophys.*, *6*, 635–642.

Sastri, J. H., N. Jyoti, V. V. Somayajulu, H. Chandra, and C. V. Devasia (2000), Ionospheric storm of early November 1993 in the Indian equatorial region, *J. Geophys. Res.*, *105*, 18,443–18,455, doi:10.1029/1999JA000372.

Scherliess, L., and B. G. Fejer (1997), Storm time dependence of equatorial disturbance dynamo zonal electric fields, *J. Geophys. Res.*, *102*, 24,037–24,046, doi:10.1029/97JA02165.

Shreedevi, P. R., S. V. Thampi, D. Chakrabarty, R. K. Choudhary, T. K. Pant, A. Bhardwaj, and S. Mukherjee (2016), On the latitudinal changes in ionospheric electrodynamics and composition based on observations over the 76–77°E meridian from both hemispheres during a geomagnetic storm, *J. Geophys. Res. Space Physics*, *121*, 1557–1568, doi:10.1002/2015JA021841.

Sobral, J. H. A., M. A. Abdu, C. S. Yamashita, W. D. Gonzalez, A. C. de Gonzalez, I. S. Batista, C. J. Zamlutti, and B. T. Tsurutani (2001), Responses of the low-latitude ionosphere to very intense geomagnetic storms, *J. Atmos. Sol. Terr. Phys.*, *63*, 965–974, doi:10.1016/S1364-6826(00)00197-8.

Sreeja, V., N. Balan, S. Ravindran, T. K. Pant, R. Sridharan, and G. J. Bailey (2009), Additional stratifications in the equatorial F region at dawn and dusk during geomagnetic storms: Role of electrodynamics, *J. Geophys. Res.*, *114*, A08309, doi:10.1029/2009JA014373.

Sreeja, V., S. Ravindran, and T. K. Pant (2010), Features of the F3 layer occurrence over the equatorial location of Trivandrum, *Ann. Geophys.*, *28*, 1741–1747, doi:10.5194/angeo-28-1741-2010.

Suvorova, A. V., C.-M. Huang, H. Matsumoto, A. V. Dmitriev, V. E. Kunitsyn, E. S. Andreeva, I. A. Nesterov, and L.-C. Tsai (2014), Low-latitude ionospheric effects of energetic electrons during a recurrent magnetic storm, *J. Geophys. Res. Space Physics*, *119*, 9283–9302, doi:10.1002/2014JA020349.

Thomas, E. G., J. B. H. Baker, J. M. Ruohoniemi, A. J. Coster, and S.-R. Zhang (2016), The geomagnetic storm time response of GPS total electron content in the North American sector, *J. Geophys. Res. Space Physics*, *121*, 1744–1759, doi:10.1002/2015JA022182.

Tulasi Ram, S., et al. (2016), Duskside enhancement of equatorial zonal electric field response to convection electric fields during the St. Patrick's Day storm on 17 March 2015, *J. Geophys. Res. Space Physics*, *121*, 538–548, doi:10.1002/2015JA021932.

Upadhayaya, A. K., S. Gupta, and P. S. Brahmanandam (2016), F2 region response to geomagnetic disturbances across Indian latitudes: O(1S) dayglow emission, *J. Geophys. Res. Space Physics*, *121*, 2595–2620, doi:10.1002/2015JA021366.

Wanliss, J. A., and K. M. Showalter (2006), High-resolution global storm index: Dst versus SYM-H, *J. Geophys. Res.*, *111*, A02202, doi:10.1029/2005JA011034.

Wei, Y., W. Wan, Z. Pu, M. Hong, Q. Zong, J. Guo, B. Zhao, and Z. Ren (2011), The transition to overshielding after sharp and gradual interplanetary magnetic field northward turning, *J. Geophys. Res.*, *116*, A01211, doi:10.1029/2010JA015985.

Wei, Y., B. Zhao, G. Li, and W. Wan (2015), Electric field penetration into Earth's ionosphere: A brief review for 2000–2013, *Sci. Bull.*, *60*(8), 748–761, doi:10.1007/s11434-015-0749-4.

Zain, A. F. M., S. Abdullah, M. J. Homam, F. C. Seman, M. Abdullah, and Y. H. Ho (2008), Observations of the F3-layer at equatorial region during 2005, *J. Atmos. Sol. Terr. Phys.*, *70*, 918–925, doi:10.1016/j.jastp.2007.12.002.

Zhang, R., L. Liu, H. Le, and Y. Chen (2016), Evidence and effects of the sunrise enhancement of the equatorial vertical plasma drift in the F region ionosphere, *J. Geophys. Res. Space Physics*, *121*, 4826–4834, doi:10.1002/2016JA022491.

Zhao, B., W. Wan, and L. Liu (2005), Responses of equatorial anomaly to the October–November 2003 superstorms, *Ann. Geophys.*, *23*, 693–706, doi:10.5194/angeo-23-693-2005.

Zhao, B., W. Wan, B. Reinisch, X. Yue, H. Le, J. Liu, and B. Xiong (2011), Features of the F3 layer in the low-latitude ionosphere at sunset, *J. Geophys. Res.*, *116*, A01313, doi:10.1029/2010JA016111.

Zhao, B., J. Zhu, B. Xiong, X. Yue, M. Zhang, M. Wang, and W. Wan (2014), An empirical model of the occurrence of an additional layer in the ionosphere from the occultation technique: Preliminary results, *J. Geophys. Res. Space Physics*, *119*, 10,204–10,218, doi:10.1002/2014JA020220.